New Quaternary Thiostannates and Thiogermanates $A_2Hg_3M_2S_8$ (A = Cs, Rb; M = Sn, Ge) through Molten A_2S_x. Reversible Glass Formation in $Cs_2Hg_3M_2S_8$

Gregory A. Marking, Jason A. Hanko, and Mercouri G. Kanatzidis*

Department of Chemistry and the Center for Fundamental Materials Research, Michigan State University, East Lansing, Michigan 48824

Received December 16, 1997. Revised Manuscript Received February 16, 1998

$Cs_2Hg_3M_2S_8$ (M = Ge, Sn) were synthesized in 70% and 65% yields by reacting HgS, and Sn or Ge, in molten Cs_2S_x at 520 °C. $Rb_2Hg_3Sn_2S_8$ and $Rb_2Hg_3Ge_2S_8$ were synthesized in 42% and 73% yield by reacting the same reagents in molten Rb_2S_x at 350 °C. $Cs_2Hg_3M_2S_8$ crystallize in the triclinic space group $P\bar{1}$. $Cs_2Hg_3Sn_2S_8$: $a = 7.878(2)$ Å, $b = 9.157(3)$ Å, $c = 6.803(2)$ Å, $\alpha = 92.96(2)°$, $\beta = 109.45(2)°$, $\gamma = 107.81(2)°$, $V = 434.1(2)$ Å^3, and $D_{calc} = 5.207$ g/cm^3. The unit cell of isostructural $Cs_2Hg_3Ge_2S_8$ is $a = 7.808(2)$ Å, $b = 9.164(2)$ Å, $c = 6.612(2)$ Å, $\alpha = 92.02(2)°$, $\beta = 108.65(2)°$g, $\gamma = 108.10(2)°$, and $V = 419.9(2)$ Å^3. $Rb_2Hg_3M_2S_8$ crystallize in the monoclinic space group $P2_1/c$, $Rb_2Hg_3Sn_2S_8$: $a = 10.132(2)$ Å, $b = 6.540(2)$ Å, $c = 13.434(2)$ Å, $\beta = 97.93(1)°$, $V = 881.7(6)$ Å^3, and $D_{calc} = 4.770$ g/cm^3. The unit cell of isostructural $Rb_2Hg_3Ge_2S_8$ is $a = 9.938$ (3) Å, $b = 6.352$ (2) Å, $c = 13.117$ (3) Å, $\beta = 97.33$ (2)°, and $V = 821.3$ (4) Å^3. The structure of $Cs_2Hg_3M_2S_8$ consists of $[Hg_3M_2S_8]^{2-}$ layers separated by Cs^+ cations. The layers contain tetrahedral Sn^{4+} or Ge^{4+} centers and two types of Hg^{2+}, two coordinate linear and three-coordinate pseudotrigonal centers. The structure of $Rb_2Hg_3M_2S_8$ consists of a 3-dimensional $[Hg_3M_2S_8]^{2-}$ framework with Rb^+ cations located within channels of the structure. This structure also contains tetrahedral Sn^{4+} or Ge^{4+} centers and two types of Hg^{2+}, the two-coordinate linear type and a four-coordinate "seesaw" geometry. Optical band gaps, determined from single-crystal UV/vis spectroscopy, range from 2.52 eV in the tin-based compounds to 2.89 eV in the germanium-based analogues. $Cs_2Hg_3M_2S_8$ become glasses upon melting. Infrared and Raman spectroscopic characterization of the glasses are reported.

Introduction

The synthetic chemistry of thiogermanates and thiostannates has been extensively investigated using high-temperature solid-state[1] and low-temperature solvothermal[2] techniques. Many of the materials found in these investigations contain tetrahedral (thio-, selenometalates) $[GeS_4]^{4-}$ and $[SnS_4]^{4-}$ ligands that bridge a variety of different metal centers into extended structures. Isolated $[GeS_4]^{4-}$ and $[SnS_4]^{4-}$ tetrahedra are found in many compounds such as Pb_2GeS_4[3] and $Na_4SnS_4 \cdot 14H_2O$.[4] $[MS_4]^{4-}$ tetrahedra often condense forming larger dimeric and/or polymeric units. Two tetrahedra can share an edge, forming $[M_2S_6]^{4-}$ dimer which can be found as isolated units in $Na_4Ge_2S_6 \cdot 14H_2O$[5] and as fragments of a larger structure in compounds such as $K_2Sn_2S_8$.[6] Two of these tetrahedra can also condense through the sharing of one corner, forming an $[M_2S_7]^{6-}$ unit such as that found in $Na_6Sn_2S_7$.[7] Larger adamantane-like polyhedral units $[M_4S_{10}]^{4-}$ are found in compounds including $Cs_4Ge_4S_{10} \cdot 3H_2O$[8] and still larger polymeric condensation units are known.[1] In addition to those based on a tetrahedron, other thiogermanate and thiostannate ligands are known. $[Ge_2S_6]^{6-}$ ethane-like dumbbell ligands are found in compounds such as $K_6Ge_2S_6$[9] and $Na_8Pb_2[Ge_2S_6]_2$.[10] Trigonal bipyramidal $[SnS_5]^{6-}$ fragments are found as parts of larger structures in many ternary tin compounds.[6]

Various approaches to the synthesis of thiogermanates and thiostannates had been thoroughly explored leading in part to the materials discussed above, but they had not yet been systematically studied using the molten alkali-metal polychalcogenide flux technique. Because this method has been used in recent years to prepare a wide variety of new ternary and quaternary alkali-metal thiometalates,[11] we began intensive investigations of tin and germanium quaternary alkali-metal thiometalates. Our early studies in the thiogermanate

(1) Krebs, B. *Angew. Chem., Int. Ed. Engl.* **1983**, *22*, 113.
(2) Olivier-Fourcade, J.; Jumas, J. C.; Ribes, M.; Philippot, E.; Maurin, M. *J. Solid State Chem.* **1978**, *23*, 155.
(3) Susa, K.; Steinfink, H. *J. Solid State Chem.* **1971**, *7*, 75.
(4) Schiwy, W.; Pohl, S.; Krebs, B. *Z. Anorg. Allg. Chem.* **1973**, *402*, 77.
(5) Krebs, B.; Pohl, S.; Schiwy, W. *Z. Anorg. Allg. Chem.* **1972**, *393*, 241.
(6) Liao, J.-H.; Varotsis, C.; Kanatzidis, M. G. *Inorg. Chem.* **1993**, *32*, 2453.
(7) Krebs, B.; Schiwy, W. Z. *Z. Anorg. Allg. Chem.* **1973**, *393*, 63.
(8) Pohl, S.; Krebs, B. Z. *Anorg. Allg. Chem.* **1976**, *424*, 265.
(9) Eisenmann, B.; Kieselbach, E.; Schäfer, H.; Schrod, H. *Z. Anorg. Allg. Chem.* **1984**, *516*, 49.
(10) Marking, G. A.; Kanatzidis, M. G. *J. Alloys Compounds* **1997**, *259*, 122.
(11) Kanatzidis, M. G.; Sutorik, A. C. *Prog. Inorg. Chem.* **1995**, *43*, 151.

S0897-4756(97)00804-1 CCC: $15.00
Published on Web 03/27/1998

systems led to synthesis of the new compounds: $Rb_2PbGe_2S_6$, $K_2PbGe_2S_6$, $K_2Pb_3Ge_3S_{10}$, $Cs_4Pb_4Ge_5S_{16}$, and $K_4Sn_3Ge_3S_{14}$.[12] Further investigations resulted in the discovery of a series of novel compounds with the staggered ethane-like $[Ge_2S_6]^{6-}$ and $[Si_2S_6]^{6-}$ anions which are members of a potentially large class of new quaternary chalcogermanates and chalcosilicates[10] bridging the gap between the ternary alkali-metal chalcogermanates and chalcosilicates such as $K_6Ge_2S_6$,[9] K_3SiTe_3,[13] $Na_6Si_2Se_6$[14], and other similar compounds[15] and ternary transition-metal chalcogermanates and chalcosilicates such as $Cr_2Ge_2Te_6$,[16] $M_2Si_2Te_6$ (M = Cr, Al, Sc, In),[17] and a small number of transition-metal selenosilicates $M_2Si_2Se_6$ (V, Cr, Mn, Fe, Co, Ni) possessing CdI_2 type structures.[18]

Further investigation into the quaternary chemistry of thiostannate and thiogermanate anions using the molten alkali-metal polychalcogenide flux technique was aimed at incorporating mercury into the syntheses. Mercury is a large polarizable main-group metal with a considerable potential to form interesting new structures due to its variable coordination preference (e.g., 2, 3, 4) and it has already been shown to be amenable to this synthetic technique. The preparations of ternary compounds $K_2Hg_3Q_4$[19] and $K_2Hg_6Q_7$,[19] and K_6HgQ_4[20] (Q = S, Se),[19] and the quaternary compound $BaHgSnS_4$[21] indicate that HgQ need not be an intractable thermodynamic sink during solid-state syntheses. In addition, tin has long been known to form many of the same chalcometalate ligands as does germanium, and it too has been shown to be amenable to the molten alkali-metal polychalcogenide flux synthetic technique. Ternary tin compounds such as $K_2Sn_2S_8$, α,β-$Rb_2Sn_2S_8$, $Cs_2Sn_2S_6$, Cs_2SnS_{14},[6] $Cs_2Sn_3S_7 \cdot {}^1/_2S_8$,[22] and others have been prepared, so we decided to incorporate thiostannate ligands along with thiogermanates into our investigations of mercury. It is noteworthy that the new quaternaries $K_2Y_4Sn_2S_{11}$[23] and $CsSmGeS_4$[24] have recently been prepared through a nearly direct combination reaction and an interesting alkali halide flux technique, respectively. Here we report the results of these investigations that led to the syntheses of the new phase $Cs_2Hg_3M_2S_8$ (M = Ge, Sn) and γ-$Rb_2Hg_3M_2S_8$ (M = Ge, Sn) using molten Cs_2S_x and Rb_2S_x fluxes. Additional results including $Rb_2HgSn_2S_8$, α,β-$K_2Hg_3M_2S_8$, and β-$Rb_2Hg_3M_2S_8$ will be forthcoming.[25] The Cs compounds exhibit glass forming properties, a rare occurrence among *stoichiometric* chalcogenide compounds.

Experimental Section

Synthesis. All manipulations were carried out under a nitrogen atmosphere. Reagents were used as obtained: (i) red HgS, powder, Alfa-Aesar, Ward Hill, MA; (ii) Sn metal, 99.8%, −325 mesh, Cerac, Milwaukee, WI; (iii) Ge metal, 99.999%, −100 mesh, Alfa-Aesar, Ward Hill, MA; (iv) sulfur powder, sublimed, Spectrum, Gardena, CA; (v) cesium metal, 99.98%, Cerac, Milwaukee, WI; (vi) rubidium metal, 99.8%, Cerac, Milwaukee, WI. Cs_2S and Rb_2S were prepared using a modified literature procedure.[26]

Bright yellow crystals of $Cs_2Hg_3Sn_2S_8$ (**I**), yellow-orange crystals of $Cs_2Hg_3Ge_2S_8$ (**II**), yellow crystals of $Rb_2Hg_3Sn_2S_8$ (**III**), and pale yellow-brown crystals of $Rb_2Hg_3Ge_2S_8$ (**IV**) are formed through sulfur-rich "low basic"[11] flux reactions. All products are stable in water and other common solvents. No decomposition was detected in samples left under ambient atmospheric conditions for periods up to and exceeding 2 years. Compound **I** can be prepared with >95% phase purity in an approximate 70% yield (based on Sn) by heating a mixture of $4Cs_2S + 5HgS + 2Sn + 32S$ at 520 °C for 4 days and slowly cooling to 180 °C over 80 h. The excess HgS minimizes formation of competing phases, $Cs_2HgSn_3S_8$[25b] and others, and the remainder of the reaction mixture dissolves in polar solvents such as dimethylformamide, methanol, or water. Compound **II** is prepared as the major product with >70% phase purity and an approximate 65% yield (based on Ge) using a synthesis identical to that used for **I** with the sole difference, Sn metal was replaced by Ge metal. Compound **III** can be prepared as a pure phase in 42% yield (based on Sn) by heating a mixture of $4Rb_2S + 4.5HgS + 2Sn + 32S$ at 350 °C for 4 days and slowly cooling to 152 °C over 99 h. Compound **IV** is also prepared as a pure phase with a 73% yield using the same method as that used for **III** using Ge.

Semiquantitative analyses of **I**−**IV**, using SEM-EDS, showed their compositions to be consistent with the expected formulas. X-ray powder diffraction experiments indicated that **I** and **II** were isostructural, as were **III** and **IV**. The homogeneities of all four phases were confirmed by comparison of observed X-ray powder diffraction patterns to those calculated from single-crystal refinement or unit cell data.

Physical Measurements. Semiquantitative microprobe analyses were performed with a JEOL JSM-6400V scanning electron microscope (SEM) equipped with a Tracor Northern energy-dispersive spectroscope (EDS) detector. Data acquisitions were performed using an accelerating voltage of 20 kV and a 20 or 30 s accumulation time. Powder X-ray diffraction (XRD) was performed using a calibrated Phillips XRD-3000 controlled by a PDP 11 computer using Ni-filtered Cu radiation and operating at 40 kV and 20 mA. Calculated X-ray powder patterns used for comparative purposes were obtained using Cerius[2] software.[27]

Raman spectra were recorded using a BIO-RAD FT Raman spectrometer with a Spectra-Physics Topaz T10-106c laser. FT-IR spectra were recorded for these compounds as solids in a CsI matrix. Data were recorded from the far-IR region (600−50 cm^{-1}, 4 cm^{-1} resolution) with the use of a Nicolet 750 FT-IR spectrometer equipped with a DTGS/PE detector and a solid substrate beam splitter.

Optical transmission measurements were made at room temperature on single crystals using a Hitachi U-6000 micro-

(12) Marking, G. A.; Kanatzidis, M. G., manuscript in preparation.
(13) (a) Dittmar, G. *Acta Crystallogr.* **1978**, *B34*, 2390. (b) Dittmar, G. *Angew. Chem.* **1977**, *89*, 566.
(14) Feltz, A.; Pfaff, G. *Z. Chem.* **1983**, *23*, 68.
(15) (a) Dittmar, G. *Z. Anorg. Allg. Chem.* **1978**, *453*, 68. (b) Eisenmann, B.; Hansa, J.; Schäfer, H. *Mater. Res. Bull.* **1985**, *20*, 1339.
(16) Carteaux, V.; Brunet, D.; Ouvrard, G.; Andre, G.; M. *J. Phys.: Condens. Matter* **1995**, *7*, 69−87.
(17) (a) Ouvrard, G.; Sandre, E.; Brec, R. *J. Solid State Chem.* **1988**, *73*, 27. (b) Sandre, E.; Carteaux, V.; Ouvrard, V. *C. R. Acad. Sci. Paris* **1992**, *314*, 1151. (c) Sandre, E.; Carteaux, V.; Marie, A. M.; Ouvrard. G. *J. Alloys Compounds* **1994**, *204*, 145.
(18) Gopalakrishnan, J.; Nanjundaswamy, K. S. *Mater. Res. Bull.* **1988**, *23*, 107.
(19) (a) Kanatzidis, M. G.; Park, Y. *Chem. Mater.* **1990**, *2*, 99−101. (b) Axtell, E. A., III; Park, Y.; Chondroudis, K.; Kanatzidis, M. G. *J. Am. Chem. Soc.* **1998**, *120*, 124−136.
(20) Sommer, H.; Hoppe, R. Z. *Z. Anorg. Allg. Chem.* **1978**, *443*, 201.
(21) Teske, C. L. *Z. Naturforsch.* **1980**, *35B*, 7−11.
(22) Marking, G. A.; Kanatzidis, M. G. *Chem. Mater.* **1995**, *7*, 1915.
(23) Wu, P.; Ibers, J. A. *J. Solid State Chem.* **1994**, *110*, 156.
(24) Bucher, C. K.; Hwu, S.-J. *Inorg. Chem.* **1994**, *33*, 5831.
(25) (a) Marking, G. A.; Liao, J.-H.; Kanatzidis, M. G., manuscript in preparation. (b) Liao, J.-H. Ph.D. Dissertation, Michigan State University, 1993. (c) Kanatzidis, M. G.; Liao, J.-H.; Marking, G. A. United States Patent 5,618,471, 1997. (d) Kanatzidis, M. G.; Liao, J.-H.; Marking, G. A. United States Patent 5,614,128, 1997.
(26) Feher, F. *Handbuch der Praparativen Anorganischen Chemie*; Brauer, G., Ed.; Ferdinand Enke: Stuttgart, Germany, 1954; pp 280−281.
(27) CERIUS[2], Version 2.0, Molecular Simulations Inc., Cambridge, England, 1995.

scopic FT spectrophotometer with an Olympus BH-2 metallurgical microscope over the range 380−900 nm.

Differential thermal analyses (DTA) were performed using a computer-controlled Shimadzu DTA-50 thermal analyzer. A 38 mg sample of **I**, 33 mg samples of **II** and **IV**, and a 51 mg sample of **III** were sealed in quartz tubes under vacuum and then heated at 10 °C/min to temperatures of 650 °C for **I**, **III**, and **IV** and 700 °C for **II**, isothermed from 10 min, and finally cooled to 100 °C at 10 °C/min. These experiments were repeated through two heating and cooling cycles, and empty sealed quartz tubes of approximately the same mass as the sample tubes were present on the reference side of the detector during measurements.

X-ray Crystallography. Single crystals of the two Sn phases **I** and **III** were mounted on glass fibers and intensity data sets were collected using a Rigaku AFC6S diffractometer with graphite monochromated Mo Kα radiation operating at 50 kV and 30 mA at 23 °C. Three standard reflections were monitored every 300 reflections for each crystal and indicated that no significant decay occurred. A hemisphere of diffraction data ($+hk+l$, $-hk+l$, $+hk-l$, $-hk-l$) were collected out to 50° in 2θ for **I** and two octants of data ($hk+l$, $hk-l$) were collected out to 50° in 2θ for **III** using $2\theta-\omega$ scans. The structures were solved using SHELXS-86[28] direct methods and refined with the TEXSAN[29] package of crystallographic software.

An empirical absorption correction based on ψ-scans was applied to the data, followed by a DIFABS[30] correction to the isotropically refined structure. All equivalent reflections were averaged after absorption correction. After complete anisotropic refinement, the R/R_w's were 3.9%/4.7% for **I** and 3.4%/4.1% for **III**. Unit cell parameters and Laue symmetries for the Ge analogues **II** and **IV** were obtained for crystals mounted on glass fibers using a Rigaku AFC6S diffractometer with graphite monochromated Mo Kα radiation operating at 50 kV and 30 mA at 23 °C. Tables 1−3 contain pertinent crystallographic data, results, and atomic parameters.

Results and Discussion

Structure. $Cs_2Hg_3Sn_2S_8$ (**I**) and $Cs_2Hg_3Ge_2S_8$ (**II**) are X-ray isomorphous. This structure contains $[Hg_3M_2S_8]^{2-}$ layers with Cs^+ cations located between the layers as shown in Figure 1. Pseudotrigonal HgS_3 and tetrahedral $[MS_4]^{4-}$ units alternate forming eight-membered −S−Hg−S−M−S−Hg−S−M− rings that have chairlike conformation. There are two distinct eight-membered rings which alternate sharing Hg−S−M edges with each other and forming $[Hg_2M_2S_8]^{4-}$ double chains of condensed rings running along the *c*-axis. Two sulfur atoms per ring would extend terminally from the tetrahedral M centers if these chains were isolated, but instead, these sulfur atoms bridge Hg positions between the chains forming linear HgS_2 units that link the "chains" into $[Hg_3M_2S_8]^{2-}$ layers lying perpendicular to the *a*-axis. The chains of alternating eight-membered rings composed of pseudotrigonal HgS_3 and SnS_4 units and the linear HgS_2 units connecting them can clearly be seen in the single $[Hg_3M_2S_8]^{2-}$ layer depicted in Figure 2. Two of the distinct but adjacent eight-membered rings that form the "chains" running along the *c* axis are shown in Figure 3. The dotted lines in this figure represent the folds in the nearly ideal chairlike conformation of one ring. The chairlike geometry of the second ring is also evident but is considerably less perfect than that of the first ring.

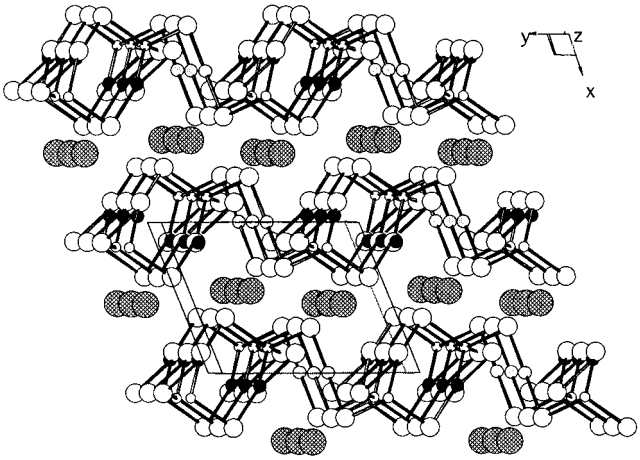

Figure 1. View parallel to the *c*-axis of $Cs_2Hg_3M_2S_8$ showing the stacking of the layers and placement of Cs^+ cations. Large open circles are S atoms, black circles are 3-coordinate Hg atoms, small shaded circles are 2-coordinate Hg atoms, small open circles are M = Ge, Sn atoms, and large shaded circles are Cs atoms.

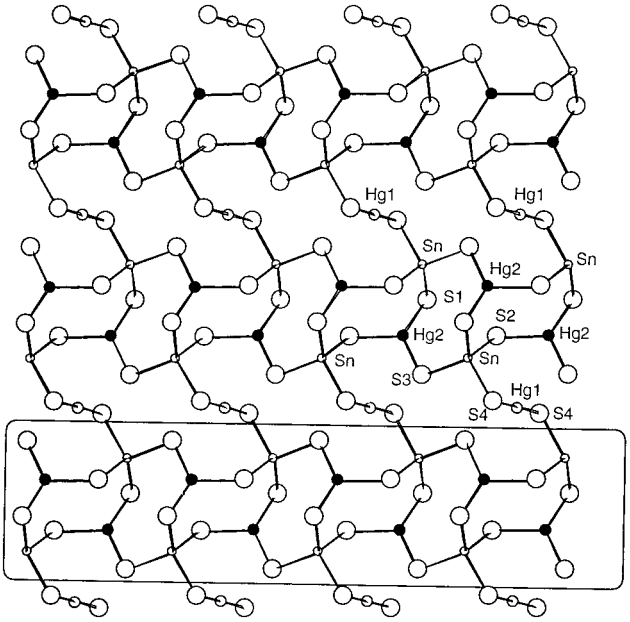

Figure 2. View perpendicular to the *a*-axis of $Cs_2Hg_3M_2S_8$ showing a $[Hg_3M_2S_8]^{2-}$ layer. The pseudotrigonal and linear Hg centers are clearly evident. The boxed area is meant to highlight the $[Hg_2M_2S_8]^{4-}$ double chains.

The tetrahedral geometry of the $[SnS_4]^{4-}$ unit in $Cs_2Hg_3Sn_2S_8$ is relatively undistorted, with Sn−S bond distances ranging from 2.386(5) to 2.425(4) Å and the S−Sn−S bond angles from 103.7(2) to 112.8(2)°. The HgS_2 unit is strictly linear with Hg1 located on an inversion center, with a Hg−S bond distance of 2.345(5) Å and a S−Hg−S bond angle of 180°. The pseudotrigonal HgS_3 unit is severely distorted from the ideal trigonal geometry. The three Hg−S bond distances are 2.422(5), 2.487(5), and 2.547(5) Å while the three S−Hg−S bond angles are 86.2(1), 104.4(1), and 132.9(2)°. The largest bond angle is between the two shortest Hg−S contacts, and the smallest bond angle is between the two longest Hg−S contacts. The Hg position is 0.239 Å out of the plane formed by the three sulfurs. There

(28) Sheldrick, G. M. In *Crystallographic Computing 3*; Sheldrick, G. M., Kruger, C., Goddard, R., Eds.; Oxford University Press: Oxford, U.K., 1985; pp 175−189.

(29) TEXSAN: Single-Crystal Structure Analysis Software, Version 5.0, Molecular Structure Corp., The Woodlands, TX.

(30) DIFABS: An Empirical Method for Correcting Diffractometer Data for Absorption Effects; Walker, N.; Stuart, D. *Acta Crystallogr.* **1983**, *A39*, 158.

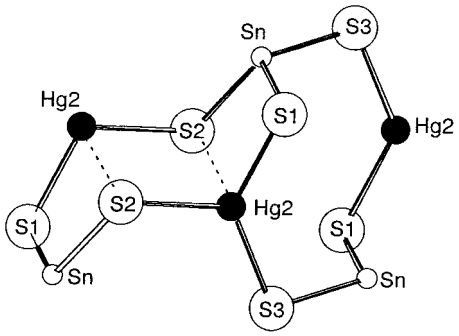

Figure 3. Two of the distinct but adjacent eight-membered rings found in $Cs_2Hg_3M_2S_8$ are isolated in this view. The dotted lines represent the folds in the chairlike conformation of one ring.

Table 1. Unit Cell Parameters for $Cs_2Hg_3Sn_2S_8$, $Cs_2Hg_3Ge_2S_8$, $Rb_2Hg_3Sn_2S_8$, and $Rb_2Hg_3Ge_2S_8$

formula	$Cs_2Hg_3Sn_2S_8$	$Cs_2Hg_3Ge_2S_8$	$Rb_2Hg_3Sn_2S_8$	$Rb_2Hg_3Ge_2S_8$
space group	$P\bar{1}$ (No. 2)	$P\bar{1}$ (No. 2)	$P2_1/c$ (No. 14)	$P2_1/c$ (No. 14)
a, Å	7.878(2)	7.808(2)	10.132(2)	9.938(3)
b, Å	9.157(3)	9.164(2)	6.540(2)	6.352(2)
c, Å	6.803(2)	6.612(2)	13.434(2)	13.117(3)
α, deg	92.96(2)	92.02(2)	90.0	90.0
β, deg	109.45(2)	108.65(2)	97.93(1)	97.33(2)
γ, deg	107.81(2)	108.10(2)	90.0	90.0
Z, V (Å^3)	1, 434.1(2)	1, 419.9(2)	2, 881.7(6)	2, 821.3(4)

Table 2. Single-Crystal Data for $Cs_2Hg_3Sn_2S_8$ and $Rb_2Hg_3Sn_2S_8$

formula	$Cs_2Hg_3Sn_2S_8$	$Rb_2Hg_3Sn_2S_8$
fw	1361.44	1266.56
d_{calc} (g/cm^3)	5.207	4.770
crystal size, mm^3	0.10 × 0.13 × 0.28	0.10 × 0.16 × 0.21
temp (°C)	23	23
radiation	Mo Kα	Mo Kα
μ (Mo Kα), cm^{-1}	342.88	350.58
secondary ext coeff (10^{-7})	10.0(7)	9.0(4)
scan mode	$2\theta-\omega$	$2\theta-\omega$
scan speed, deg/min	4	4
2θ max, deg	50	50
no. of data collected	1639	1812
no. of unique data	1518	1712
no. of data observed, $I > 3\sigma(I)$	1206	1097
no. of variables	71	71
abs correction	DIFABS	DIFABS
abs ratio (min/max)	0.3831	0.5061
R/R_w,[a] %	3.9/4.7	3.4/4.1
GOF	1.74	1.41
residual e-density (pos)	+2.207	+1.476
residual e-density (neg)	−3.008	−1.186

[a] $R = \Sigma(|F_o| - |F_c|)/\Sigma|F_o|$. $R_w = \{\Sigma w(|F_o| - |F_c|)^2/\Sigma w|F_o|^2\}^{1/2}$.

is an additional nonbonding Hg−S distance of 3.108(5) Å to Hg2 within the layer, and there is a short interlayer S−S contact of 3.19(1) Å between the $[Hg_3Sn_2S_8]^{2-}$ layers. The important interatomic distances and bond angles for **I** are listed in Table 4.

The isostructural $Rb_2Hg_3Sn_2S_8$ (**III**) and $Rb_2Hg_3Ge_2S_8$ (**IV**) differ substantially from their Cs relatives above, because instead of a two-dimensional structure they adopt a new three-dimensional $[Hg_3M_2S_8]^{2-}$ framework with Rb^+ cations located in its channels; see Figure 4. Tetrahedral $[MS_4]^{4-}$ and "seesaw" four-coordinate HgS_4 units alternate forming eight-membered rings. The two distinct types of eight-membered rings alternate sharing Hg−S−M edges forming "chains" along the *b*-axis. These "chains" are linked in two orthogonal directions as opposed to the one-directional linkage of "chains" in **I** and **II**. These chains are condensed along the *c*-axis direction by sharing the sulfur "legs" of the HgS_4 "seesaws" and forming $[Hg_2M_2S_8]^{4-}$ slabs perpendicular to the *a*-axis. These $[Hg_2M_2S_8]^{4-}$ slabs are further

Table 3. Positional Parameters and B_{eq}'s for $Cs_2Hg_3Sn_2S_8$ and $Rb_2Hg_3Sn_2S_8$

atom	x	y	z	B_{eq}
		$Cs_2Hg_3Sn_2S_8$		
Cs	0.4555(2)	0.7458(1)	0.1100(2)	1.44(4)
Hg1	0.0	0.5	0.5	0.82(3)
Hg2	0.0855(1)	0.88233(9)	0.3347(1)	1.20(3)
Sn	0.1666(2)	0.2625(1)	0.2573(2)	0.65(4)
S1	0.3630(7)	0.1039(6)	0.3347(7)	1.1(1)
S2	0.8646(7)	0.1158(6)	0.2754(7)	1.1(1)
S3	0.1340(7)	0.3470(5)	0.9239(7)	1.2(1)
S4	0.3012(3)	0.5036(5)	0.5079(7)	0.9(1)
		$Rb_2Hg_3Sn_2S_8$		
Rb	0.7196(2)	0.6646(3)	0.8065(1)	2.46(8)
Hg1	0.5	0.0	0.0	2.37(5)
Hg2	0.99723(7)	0.2041(1)	0.88107(6)	2.36(3)
Sn	0.7824(1)	0.1819(2)	0.57546(8)	1.09(4)
S1	0.0307(4)	0.8156(7)	0.8225(3)	1.7(2)
S2	0.5791(4)	0.2093(8)	0.1369(4)	2.2(2)
S3	0.2257(4)	0.3171(7)	0.9285(3)	1.8(2)
S4	0.7641(4)	0.1906(7)	0.9070(3)	1.7(2)

Table 4. Selected Interatomic Distances (Å) and Important Bond Angles (deg) for $Cs_8Hg_3Sn_2S_8$

atoms	distance	atoms	distance
Cs−S1	3.588(5)	Hg2−S1	2.487(5)
Cs−S2	3.569(5)	Hg2−S2	2.547(5)
Cs−S2	3.694(5)	Hg2−S2	3.108(5)
Cs−S3	3.617(5)	Hg2−S3	2.422(5)
Cs−S3	3.659(6)		
		Sn−S1	2.386(5)
Hg1−S4	2.345(5)	Sn−S2	2.395(5)
		Sn−S3	2.392(5)
		Sn−S4	2.425(4)
		avg. Sn−S	2.400

atoms	angle (deg)	atoms	angle (deg)
S4−Hg1−S4	180	S1−Sn−S2	107.2(2)
		S1−Sn−S3	112.4(2)
S1−Hg2−S2	86.2(1)	S1−Sn−S4	112.8(2)
S1−Hg2−S2	104.4(2)	S2−Sn−S3	112.6(2)
S1−Hg2−S3	132.9(2)	S2−Sn−S4	108.3(2)
S2−Hg2−S2	94.8(1)	S3−Sn−S4	103.7(2)
S2−Hg2−S3	104.3(2)		
S2−Hg2−S3	119.9(2)		

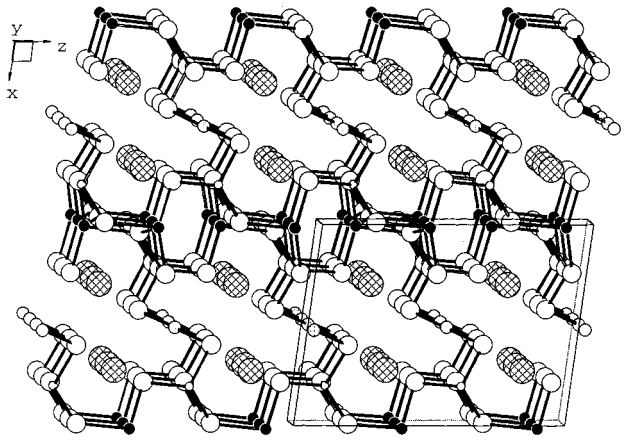

Figure 4. View down the *b*-axis direction of $Rb_2Hg_3M_2S_8$ showing the channel structure and Rb^+ cation placement within the channels. Large open circles are S atoms, black circles are 3-coordinate Hg atoms, small shaded circles are 2-coordinate Hg atoms, small open circles are M = Ge, Sn atoms, and large shaded circles are Rb atoms.

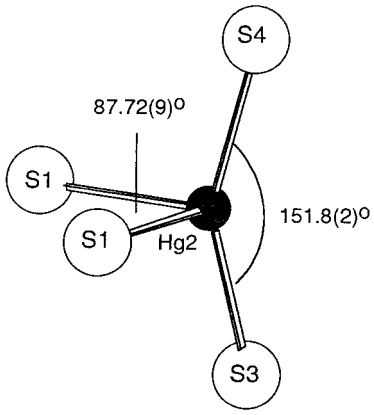

Figure 5. Geometry of the "seesaw" HgS_4 unit found in $Rb_2Hg_3M_2S_8$.

linked in the *a*-axial direction through linear HgS_2 units forming an overall three-dimensional framework with channels running along the *b*-axis. Sulfur atoms from the $[MS_4]^{4-}$ units, which would be terminal in the $[Hg_2M_2S_8]^{4-}$ slab, bridge to Hg positions forming the linear HgS_2 links between the slabs. A view down the channels along the *b*-axial direction is shown in Figure 4.

The geometry of the $[SnS_4]^{4-}$ unit is tetrahedral, with Sn−S bond distance ranging from 2.348(4) to 2.429(5) Å and S−Sn−S bond angles from 105.0(2) to 114.1(2)°. The linear Hg is on an inversion center with a Hg−S bond distance of 2.343(5) and bond angle of 180°. The "seesaw" HgS_4 unit has an interesting geometry. The Hg−S bond distances are 2.430(4), 2.436(4), 2.695(5), and 2.806(4) Å and the angle between the two shortest Hg−S contacts is 151.8(2)°. The two longer Hg−S contacts form the legs of the seesaw and have an angle of 87.72(9)° between them. The four other angles in this unit range from 98.1(1) to 102.1(1)°. A view of the "seesaw" HgS_4 unit in $Rb_2Hg_3Sn_2S_8$ is shown in Figure 5. One of the two distinct eight-membered rings in $Rb_2Hg_3Sn_2S_8$ is depicted in Figure 6. The geometry and arrangement of the alternating SnS_4 and HgS_4 units is readily apparent. Important interatomic distances and bond angles for $Rb_2Hg_3Sn_2S_8$ are listed in Table 5.

The fusion of different metal centered polyhedral fragments in an alternating fashion to form larger ringlike fragments such as those in $A_2Hg_3M_2S_8$ is found in some other systems as well. The linear HgS_2 and tetrahedral HgS_4 units found in $Cs_2Hg_3Sn_2S_8$ combine in the $K_2Hg_6S_7$[19] structure to form rings that align along one axis forming channels in a three-dimensional framework. The "seesaw" coordination of HgS_4 in $A_2Hg_3M_2S_8$ is however quite unusual. The HgS_4 fragment in $BaHgSnS_4$[21] is a severely distorted tetrahedron with some resemblance to a "seesaw" shape but the bond angle between the two shortest Hg−S contacts is only 135° in $BaHgSnS_4$, while it is substantially larger at 152° in $Rb_2Hg_3Sn_2S_8$. There are additional bond angle discrepancies between the HgS_4 polyhedral units in these two compounds.

The transition from a two-dimensional structure of the $[Hg_3M_2S_8]^{2-}$ anion in the Cs^+ salt to a three-dimensional tunnel structure in the Rb^+ analogue is understood in terms of the counterion effect.[31] This is a powerful effect that seems to control the behavior of

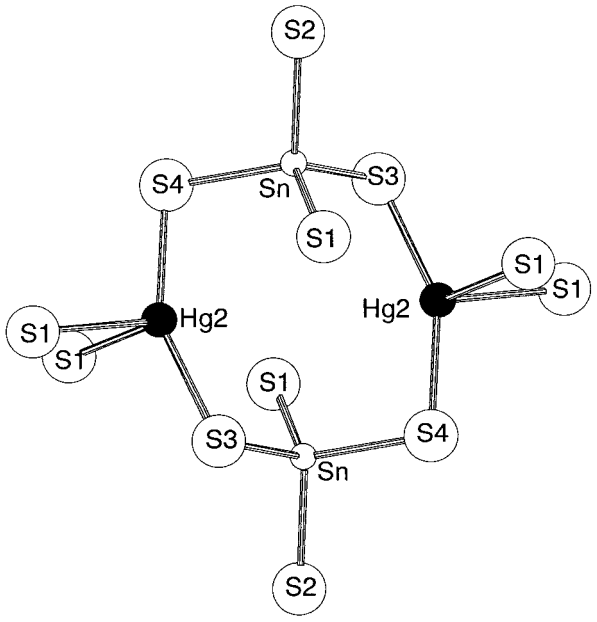

Figure 6. Geometry and arrangement of the alternating SnS_4 and HgS_4 units in one of the two distinct types of eight-membered rings found in $Rb_2Hg_3M_2S_8$.

Table 5. Selected Interatomic Distances (Å) and Important Bond Angles (deg) for $Rb_2Hg_3Sn_2S_8$

atoms	distance	atoms	distance
Rb−S1	3.281(5)	Hg2−S1	2.695(5)
Rb−S2	3.324(5)	Hg2−S1	2.806(4)
Rb−S2	3.507(5)	Hg2−S3	2.430(4)
Rb−S3	3.427(5)	Hg2−S4	2.436(4)
Rb−S3	3.529(5)		
Rb−S4	3.387(5)	Sn−S1	2.348(4)
		Sn−S2	2.429(5)
Hg1−S2	2.343(5)	Sn−S3	2.388(4)
		Sn−S4	2.394(4)
		avg. Sn−S	2.390

atoms	angle (deg)	atoms	angle (deg)
S2−Hg1−S2	180	S1−Sn−S2	110.3(2)
		S1−Sn−S3	114.1(2)
S1−Hg2−S1	87.72(9)	S1−Sn−S4	111.9(2)
S1−Hg2−S3	102.1(1)	S2−Sn−S3	105.8(2)
S1−Hg2−S3	98.1(1)	S2−Sn−S4	105.0(2)
S1−Hg2−S4	99.8(1)	S3−Sn−S4	109.2(2)
S1−Hg2−S4	100.3(1)		
S3−Hg2−S4	151.8(2)		

systems where one deals with Coulombically interacting counterions (e.g., alkali metals, organic cations, and even alkaline earths) and covalently linked anionic frameworks in the same crystal lattice. In general, the smaller the counterion is, the greater the framework's preferred dimensionality. Outstanding examples of this can also be found in many other systems such as $NaAuSe_2/KAuSe_2$,[32] NaCuTe/KCuTe,[33] and $Cs_2Cu_2P_2Se_6/K_2Cu_2P_2Se_6$.[34]

Physical Measurements. The thermal behavior of the Cs-containing materials $Cs_2Hg_3Sn_2S_8$ (**I**) and $Cs_2Hg_3Ge_2S_8$ (**II**) were found to be similar through differential thermal analysis. The DTA of **I** resulted in a

(31) For a description of the counterion effect see: Kanatzidis M. G. *Phosphorous, Silicon Sulfur* **1994**, *93−94*, 159.
(32) Park, Y., Kanatzidis, M. G. *J. Alloys Comp.* **1997**, *257*, 137.
(33) (a) Berger, R.; Eriksson, L. *J. Less-Common Met.* **1990**, *161*, 101. (b) Savelsberg, G.; Schäfer, H. *Z. Naturforsch.* **1978**, *33B*, 370. (c) Bronger, W.; Kathage, H. U. *J. Alloys Compd.* **1992**, *184*, 87.

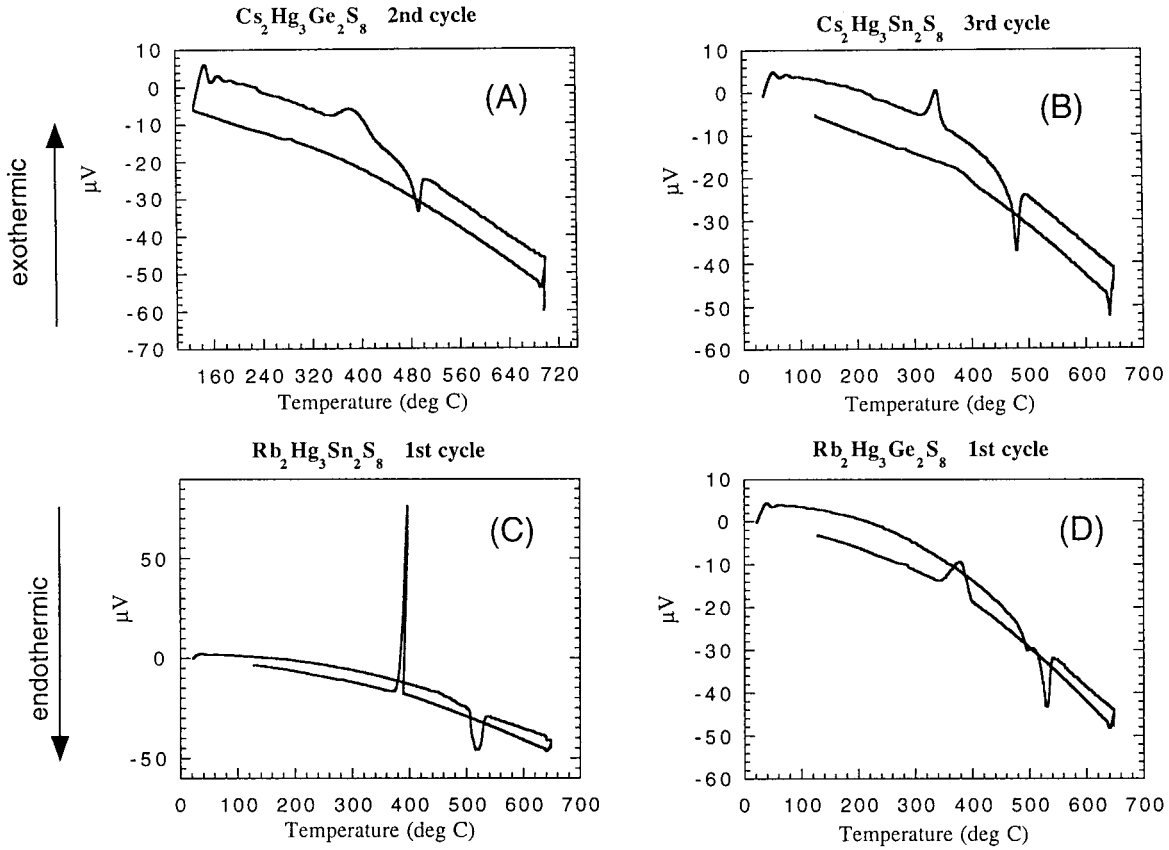

Figure 7. Differential thermal analysis data for (A) $Cs_2Hg_3Ge_2S_8$, (B) $Cs_2Hg_3Sn_2S_8$, (C) $Rb_2Hg_3Sn_2S_8$, and (D) $Rb_2Hg_3Ge_2S_8$. The Cs phases, **I** and **II**, form glasses upon cooling, and thus the second or third heating cycles are shown here. These two compounds recrystallize first and then melt again upon heating.

melting endotherm upon heating with the maximum signal centered at approximately 482 °C. The broad shoulder located on the low-temperature side of the melting endotherm was indicative of the glasslike behavior of this material. The DTA of **II** resulted in a similar melting endotherm, upon heating, centered approximately at 494 °C with a shoulder on the low-temperature side. **I** and **II** were found to form glasses upon cooling during the DTA experiments which then recrystallized at 341 and 392 °C, respectively, upon subsequent heating. This glass formation is noteworthy in that chalcogenide glasses are of interest to the scientific community involved in optics. Powder X-ray diffraction confirmed that these "glassy" materials formed upon cooling were amorphous. Powder X-ray diffraction performed on the recrystallized materials indicated that **I** melts and recrystallizes incongruently, while **II** appears to melt and recrystallize congruently. The powder pattern of **I** after DTA showed some similarity to that of the pure material before the experiment, but the presence of a second unknown phase was evident. The powder pattern of **II** after DTA appeared to be identical to that of the pure material before the experiment, but further evidence is needed to prove that **II** melts and recrystallizes congruently because the presence of an amorphous phase would not be detected through powder X-ray diffraction techniques. Another example of a stoichiometric chalcogenide compound, which also forms a glass upon melting, is $(Ph_4P)InSe_{12}$.[35] The glass-forming property of $Cs_2Hg_3M_2S_8$ (M = Ge, Sn) suggests further studies of these two materials and the exploration of fiber-forming potential.

The thermal behavior of $Rb_2Hg_3Sn_2S_8$ and $Rb_2Hg_3Ge_2S_8$ are similar to each other. The DTA of **III** resulted in an endothermic melting transition centered approximately at 519 °C upon heating and a sharp recrystallization exotherm centered at 398 °C upon cooling. The DTA of **IV** resulted in a double melting endotherm upon heating with a weak peak centered at 497 °C and a strong peak centered at 531 °C. A single broad recrystallization exotherm centered approximately at 379 °C was observed upon cooling. Both **III** and **IV** appear to melt incongruently. Although similarities exist, differences are readily apparent in the powder X-ray diffraction pattern of **III** before and after DTA. The powder X-ray diffraction pattern of **IV** is very nearly the same before and after DTA even though a double endothermic transition is observed upon melting, which suggests either that a phase transition occurs or that an amorphous phase is generated during the DTA experiment. Differential thermal analysis data collected from powdered samples of **I**, **II**, **III**, and **IV** are shown in Figure 7. DTA data obtained from the initial heating and cooling cycles of the two Rb phases, **III** and **IV**, show their melting and recrystallization behavior. DTA data obtained from subsequent heating and cooling

(34) McCarthy, T. J.; Kanatzidis, M. G. *Inorg. Chem.* **1995**, *34*, 1257.
(35) Dhingra, S.; Kanatzidis, M. G. *Science* **1992**, *258*, 1769.

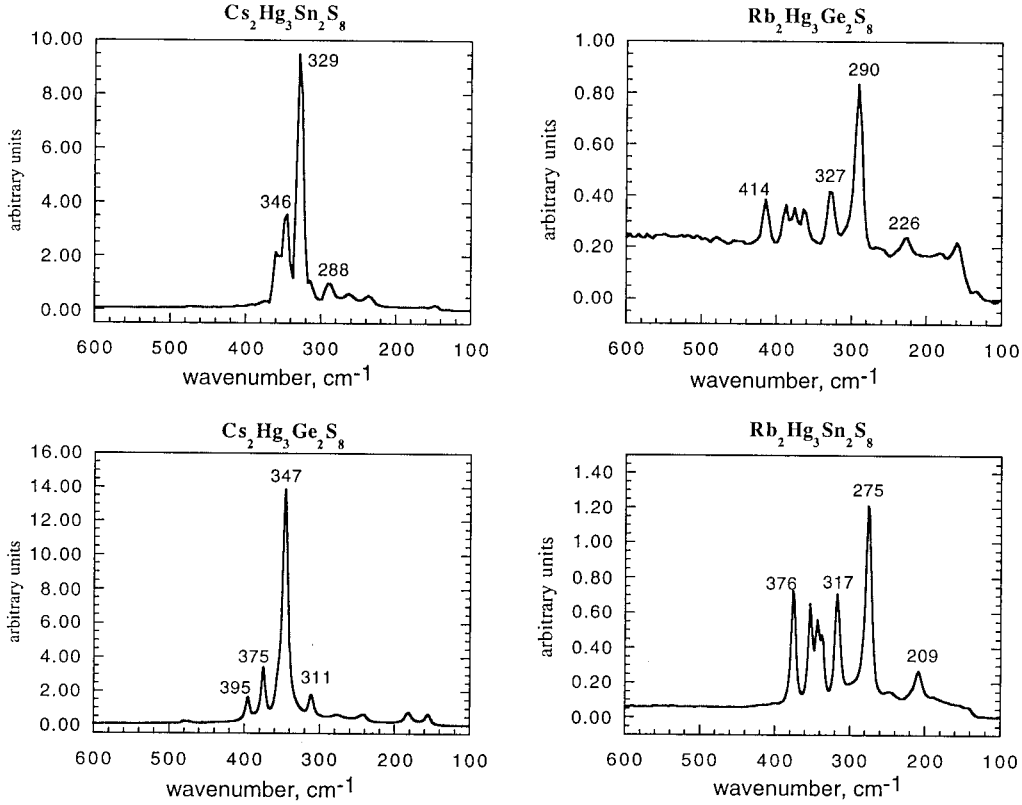

Figure 8. Fourier transform Raman spectra of all crystalline compounds.

Table 6. Raman Absorption Peaks (cm^{-1}) for $Cs_2Hg_3Sn_2S_8$, $Cs_2Hg_3Ge_2S_8$, $Rb_2Hg_3Sn_2S_8$, and $Rb_2Hg_3Ge_2S_8$

$Cs_2Hg_3Sn_2S_8$	$Cs_2Hg_3Ge_2S_8$	$Rb_2Hg_3Sn_2S_8$	$Rb_2Hg_3Ge_2S_8$
360	395	376	414
346	375	353	387
329	347	344	375
314		338	362
288	311	317	327
262	276	275	290
236	242	248	226
	182	209	158
147	156		

Table 7. Far-IR Absorption Peaks (cm^{-1}) for $Cs_2Hg_3Sn_2S_8$, $Cs_2Hg_3Ge_2S_8$, $Rb_2Hg_3Sn_2S_8$, and $Rb_2Hg_3Ge_2S_8$

$Cs_2Hg_3Sn_2S_8$	$Cs_2Hg_3Ge_2S_8$	$Rb_2Hg_3Sn_2S_8$	$Rb_2Hg_3Ge_2S_8$
363	401	388	431
357	396	382	421
340	378	353	395
335	363	349	380
288	307	341	369
262	275	328	358
234	237	284	302
	179	254	279
	169	211	229
			184

cycles of the glass-forming Cs phases, **I** and **II**, show first their recrystallization and then their melting behaviors.

Far-IR and Raman spectra show similarities between **I** and **II** and also between **III** and **IV**. A shift to higher absorption energies for the Ge phases relative to their isostructural Sn analogues is evident, but the overall pattern of the spectra remains the same within the same structural type. The absorptions above approximately 300 cm^{-1} correspond to Ge−S or Sn−S bonding interactions and are strongly affected by the specific metal, Sn or Ge. The absorptions at lower wavenumbers are less affected by the identity of the group 14 metal, and these absorptions originate primarily from Hg−S bonding interactions. Representative Raman spectra for **III** and **IV** are shown in Figure 8. Tables 6 and 7 contain lists of the most important Raman and far-IR spectroscopic absorption peaks from **I**−**IV**. The IR spectra of all four compounds from 6000 cm^{-1} to ∼500 cm^{-1} reveal a high optical transmission in this region.

The compounds reported here are wide-gap semiconductors and possess sharp optical gaps of 2.52 eV for **I**, 2.66 eV for **II**, 2.70 eV for **III**, and 2.89 eV for **IV**. The

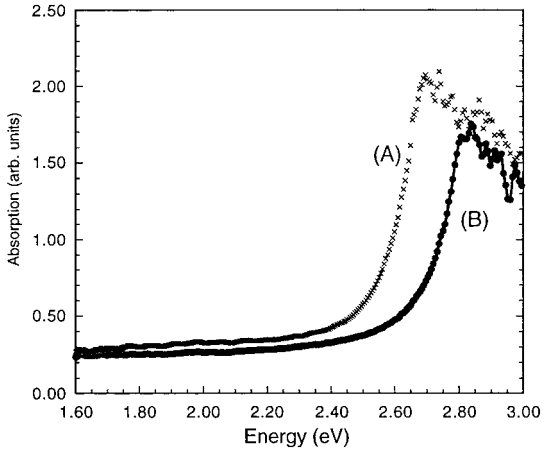

Figure 9. Single-crystal optical transmission spectra converted to absorption spectra for (A) $Cs_2Hg_3Sn_2S_8$ and (B) $Cs_2Hg_3Ge_2S_8$.

absorption spectra shown in Figure 9 are typical of the spectra collected for all four materials. The IR and UV/vis data together point to a very good transmittance of

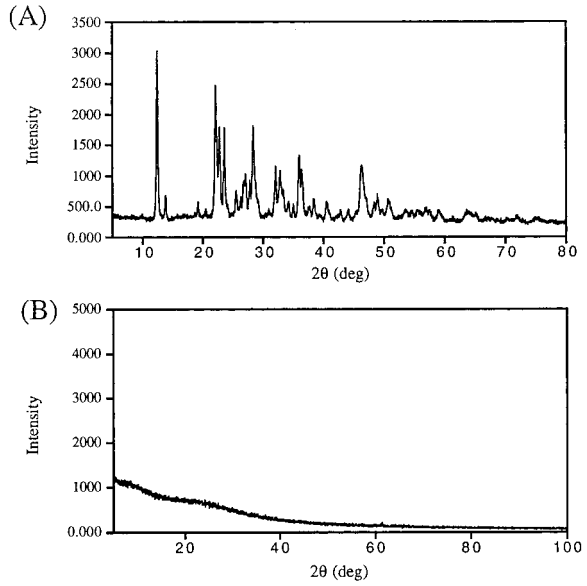

Figure 10. X-ray diffraction of (A) a polycrystalline powder sample of $Cs_2Hg_3Sn_2S_8$ and (B) a glassy powdered sample of $Cs_2Hg_3Sn_2S_8$.

these materials over a very wide spectroscopic range (~0.5−12 μm). This, coupled with the glass-forming properties of the Cs salts, stresses their possible application as low-frequency optical fibers in communications.

The higher band gap energies of the Ge compounds relative to their isostructural Sn analogues are indicative of stronger bonding forces. Their melting points follow the same trend, where the Ge compounds melt at higher temperatures than do their isostructural Sn analogues. Additionally, the three-dimensional $[Hg_3M_2S_8]^{2-}$ frameworks found in the Rb compounds are more tightly bound together than are the two-dimensional $[Hg_3M_2S_8]^{2-}$ layers found in the Cs compounds. The Rb compounds have larger band gaps and higher melting points than do the corresponding Cs compounds, and the Hg−S and Sn−S bond distances listed in Tables 4 and 5 are shorter in the Rb compound than in the Cs compound. The shorter distances, higher melting points, and larger band gaps in **III** relative to **I** correspond to higher binding energies.

The transitions responsible for these band gaps are probably charge transfer from S-based valence bands to Sn-, Ge-, and/or Hg-based conduction bands. It is unclear whether transitions from the S-based bands to the Hg-based bands and from the S-based bands to the Sn- and Ge-based bands are both occurring or if only one of these transitions is occurring.

Glass Formation. The glass-forming behavior of $Cs_2Hg_3Sn_2S_8$ was investigated by several characterization methods. The $Cs_2Hg_3Sn_2S_8$ was taken to its glassy state by heating it at 550 °C in a hermetically closed system. The resulting amber-colored glass was optically transparent and completely amorphous; see Figure 10. The optical transmission was examined with UV−vis spectroscopy, which shows that it is transparent below 1.6 eV. The spectrum is significantly broader than that of the crystalline form of the compound and shows that the glass absorbs at energies below the band gap of the crystalline solid; see Figures 9 and 11. This suggests that glassification produced a substantial number of

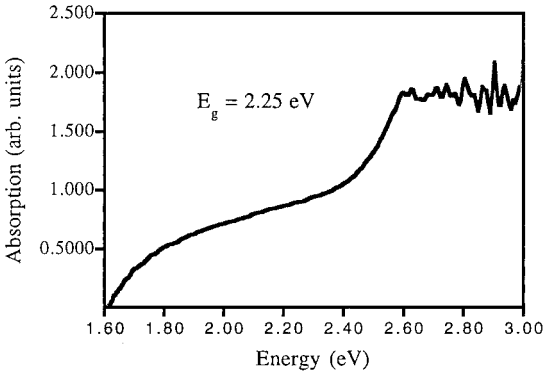

Figure 11. UV/vis optical transmission spectrum converted to absorption from a glass shard of $Cs_2Hg_3Sn_2S_8$.

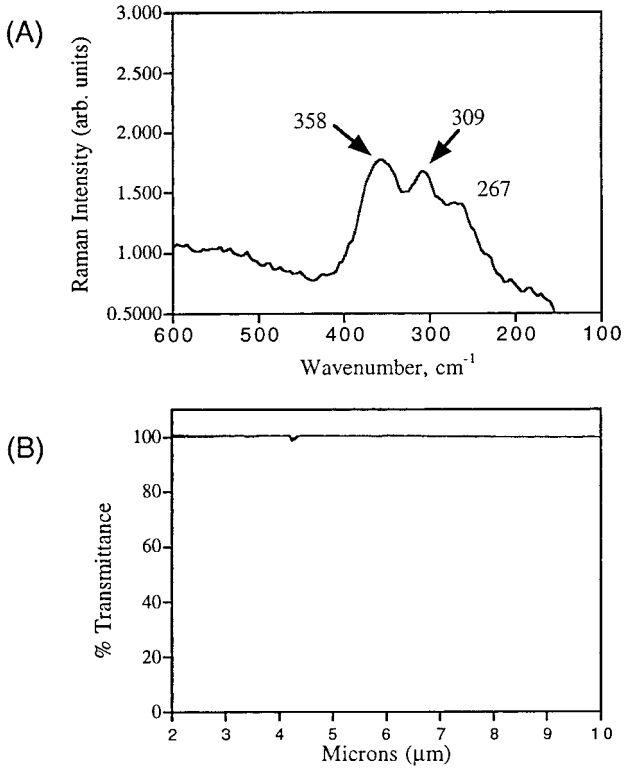

Figure 12. (A) Raman spectrum of glassy $Cs_2Hg_3Sn_2S_8$. (B) Infrared transmission spectrum from a glass shard of $Cs_2Hg_3Sn_2S_8$.

defects and mid-gap states. These defects may be associated with partial HgS loss from the sample, as supported by thermal gravimetric analysis experiments under nitrogen flow. The TGA experiments show that HgS begins to leave the sample at ~400 °C (same for $Cs_2Hg_3Ge_2S_8$). The HgS loss, which is facilitated by the flowing of gas over the sample, is quantitative, leaving $Cs_2Sn_2S_5$ behind at 600 °C. This decomposition reaction necessitates that the glass formation is carried out in a closed container. Similar considerations apply to the Ge analogue.

The Raman spectrum of the glass is also considerably broader than the corresponding spectrum of the crystalline compound, but the observed shifts occur in the same region, suggesting that key building blocks, such as the tetrahedral $[SnS_4]^{4-}$ units, are probably still intact but have lost long-range order; see Figure 12A. The infrared transparency of the glass $Cs_2Hg_3Sn_2S_8$ is remarkably good as illustrated in Figure 12B.

Conclusion

The discovery of the new quaternary compounds described in this work, containing mercury metal bound to tetrahedral $[GeS_4]^{4-}$ and $[SnS_4]^{4-}$ ligands, underscores once again the power of the molten alkali-metal polychalcogenide flux technique of synthesis. Variations of flux stoichiometry, basicity, reaction temperature, and the choices of alkali metal and main-group metal should lead to the formation of additional new structures in these systems. The use of a suitable flux to rationally construct complex framework materials from the binding of main-group and transition metals to chalcogermanate and chalcostannate ligands shows considerable promise and is currently being investigated. It is interesting that the Cs and Rb materials have such different thermal behavior although they have the same stoichiometry. The difference must derive from the variance observed in their structures. The latter arises from the cation size effect[31] where a condensed three-dimensional structure is found in the presence of the smaller Rb^+ cation while an expanded two-dimensional layered structure is found when the larger Cs^+ cation is present. The glass formation of $Cs_2Hg_3Sn_2S_8$ and $Cs_2Hg_3Ge_2S_8$ upon cooling is intriguing and unanticipated and calls for further studies of this property. The wide band gaps and high optical transmittance in the near- and mid-infrared of these two compounds suggests that further investigation is warranted to determine whether these sulfide glasses have potential for use in optical applications.

Acknowledgment. Financial support from the National Science Foundation DMR-9527347 and from Rockwell International Corp. is gratefully acknowledged. This work made use of the SEM facilities of the Center for Electron Optics, Michigan State University. M.G.K. is an A.P. Sloan Foundation and a Camille and Henry Dreyfus Teacher Scholar, 1993−1998.

Supporting Information Available: Tables of anisotropic thermal parameters of all atoms (1 page) and structure factors (F_{obs} vs F_{calc}) for **I** and **III** (19 pages). Ordering information is given on any current masthead page.

CM970804M